© AUG 2026 | IRE Journals | Volume 10 Issue 2 | ISSN: 2456-8880
DOI: https://doi.org/10.64388/IREV10I2-1722203

Multi-Dimensional Electrical Signature Analysis for Performance Monitoring and Fault Detection in Industrial Chemical Pump Systems

ADEYINKA, OLUSEGUN ALFRED[1], ALIMI, TESLIM ADEKUNLE[2], ABDULAZEEZ, KABIRU[3]
[1]*National Space Research and Development Agency (NASRDA), Obasanjo Space Centre, Abuja, Nigeria*
[2]*Department of Electrical Engineering, The Federal Polytechnic Bida, Niger State, Nigeria*
[3]*Department of Computer Engineering, Ahmadu Bello University, Zaria, Nigeria*

Abstract-* Unplanned downtime of chemical dosing and low-lift pump systems remains a major source of production loss and safety risk in industrial and municipal process plants. This paper presents a multi-dimensional electrical signature analysis (ESA) framework for continuous performance monitoring and early fault detection in a three-phase, motor-driven chemical/low-lift pump installation. High-resolution trend data comprising phase voltages, currents, total harmonic distortion (THD), active/apparent/non-active power, frequency, and power factor were logged at one-minute intervals over a representative operating window and processed to derive engineered health indicators, namely current and voltage imbalance, average current and voltage THD, calculated power factor, and reactive power ratio. Statistical process control (SPC) limits were established for phase current imbalance, and unsupervised learning — principal component analysis (PCA) combined with k-means clustering — was applied to the engineered feature space to reveal distinct operational states. The analysis identifies a dominant steady-state operating regime, a high-load/imbalance regime, and a transient start-up/shutdown regime characterized by depressed power factor and elevated harmonic distortion. Correlation analysis further shows that current harmonic distortion rises sharply as active loading falls, consistent with light-load harmonic amplification in the driven induction motor. The results demonstrate that non-invasive electrical signature analysis, combined with simple statistical and unsupervised machine-learning techniques, can provide plant engineers with an interpretable, low-cost early-warning capability for pump health monitoring without additional vibration or acoustic instrumentation.

Index Terms—* Chemical Pump, Low-Lift Pump, Electrical Signature Analysis, Condition Monitoring, Fault Detection, Power Quality, Total Harmonic Distortion, Phase Imbalance, Statistical Process Control, Principal Component Analysis, K-Means Clustering.

I. INTRODUCTION

Centrifugal chemical dosing pumps and low-lift pumps are essential components of water treatment, effluent handling, and process-chemical delivery systems, and their induction-motor drivetrains are typically expected to run continuously with minimal supervision. Unplanned failure of such units interrupts dosing accuracy, disrupts downstream processes, and, in chemical-handling contexts, can create safety and environmental hazards. Because these motors consume a large share of a plant's electrical energy and are wired directly to accessible switchgear, the electrical quantities already measured for protection and metering purposes — phase currents, voltages, harmonics, and power factor — represent an underused, non-invasive source of condition information [1], [2].

Motor current signature analysis (MCSA) has long been used to detect broken rotor bars, bearing defects, and stator winding faults from the frequency content of the stator current without physical access to the machine [1]–[4]. More recent electrical signature analysis (ESA) work extends this idea beyond the motor itself to the coupled hydraulic load, showing that current and voltage signatures can reveal impeller clogging, cavitation, seal wear, and bearing degradation in circulation and centrifugal pumps [5], [6]. In parallel, condition-monitoring research has increasingly combined classical signal features with data-driven techniques — principal component analysis (PCA), clustering, and deep learning — to summarize high-dimensional electrical and vibration data into interpretable operating states [7].

Most published pump-ESA studies, however, are conducted on small test rigs under controlled, single-fault conditions with sampling rates suited to spectral analysis. Comparatively little has been reported on how routinely logged, low-frequency SCADA/power-analyser trend data — of the kind already collected by plant power-monitoring instruments — can be mined for early warning signs during normal continuous operation. This paper addresses that gap by applying a multi-dimensional electrical signature analysis pipeline to one-minute trend data recorded from an operating three-phase chemical/low-lift pump system, combining domain-informed feature engineering, statistical process control, and unsupervised learning to characterize the machine's operating states and flag conditions that merit engineering attention.

The specific contributions of this paper are: (i) a reproducible feature-engineering scheme that converts raw power-analyser trend fields into interpretable health indicators — current/voltage imbalance, average harmonic distortion, calculated power factor, and reactive power ratio; (ii) an SPC-based control chart for phase current imbalance suitable for continuous plant deployment; (iii) an unsupervised PCA/k-means procedure that separates the pump's operating regime into normal, high-load, and transient/anomalous states without labelled fault data; and (iv) an empirical correlation analysis linking power quality degradation to loading conditions in the studied system.

II. RELATED WORK

Kliman et al. established the foundational principle that mechanical and electrical faults in induction machines imprint characteristic sidebands on the stator current spectrum, enabling non-invasive broken-rotor-bar detection without shutting the machine down [1]. Nandi, Toliyat, and Li subsequently surveyed the broader condition-monitoring literature, cataloguing current-, vibration-, and temperature-based approaches for stator, rotor, bearing, and eccentricity faults in induction motors and establishing MCSA as the dominant non-invasive technique [2]. More recently, Niu, Dong, and Chen reviewed advances in current-signature-based diagnosis for both induction and permanent-magnet synchronous motors, summarizing spectral, time–frequency, parameter-estimation, and artificial-intelligence approaches to defect detection [3], while Halder et al. focused specifically on broken-rotor-bar diagnosis techniques derived from current signatures [4].

Extending MCSA/ESA to hydraulic loads, Becker et al. demonstrated that wet-rotor circulation-pump faults — including bearing wear and impeller defects — leave detectable traces in motor current, and proposed load-point-dependent and transient current-signature indicators tailored to variable-speed pump operation [5], [6]. Sunal et al. applied transfer learning on Concordia/DQ current-pattern images collected from real, field-deployed centrifugal pumps, reporting that data-driven classification of electrical signatures can achieve useful fault-detection accuracy under real operating conditions rather than laboratory test rigs [7]. Together, this body of work confirms that electrical signals carry diagnostically useful information about both the motor and its coupled pump; however, these studies predominantly rely on high-frequency current sampling for spectral analysis of specific, pre-seeded faults.

Separately, power-quality standards such as IEEE Std 519 define acceptable limits for voltage and current total harmonic distortion at the point of common coupling, providing an established benchmark against which measured THD levels can be judged [8]. Unsupervised pattern-discovery techniques — principal component analysis for dimensionality reduction [10] and k-means clustering for partitioning multivariate observations [9] — are well established tools for summarizing such multivariate electrical and process data into a small number of interpretable operating regimes, and are adopted in this study specifically because they require no pre-labeled fault examples, which are typically unavailable for an in-service industrial pump.

© AUG 2026 | IRE Journals | Volume 10 Issue 2 | ISSN: 2456-8880
DOI: https://doi.org/10.64388/IREV10I2-1722203

III. SYSTEM DESCRIPTION AND METHODOLOGY

The proposed framework proceeds in four stages: (A) acquisition of raw three-phase electrical trend data; (B) engineering of domain-informed health indicators from the raw fields; (C) construction of a statistical process control chart for phase current imbalance; and (D) dimensionality reduction and unsupervised clustering of the engineered feature space to identify distinct operating states. Fig. 1 through Fig. 7 (Section IV) summarize the outputs of each stage as applied to the studied dataset.

A. Data Acquisition and Description

Electrical trend data were logged from a three-phase power analyser instrumented on a chemical/low-lift pump feeder over a continuous 1-minute-interval trend period, yielding 100 time-stamped observations spanning approximately 1.65 h of operation, capturing start-up, steady-state, and shutdown behaviour. Each record reports, per phase, the maximum RMS line-to-neutral and line-to-line voltage (Vrms), RMS current (Irms), voltage and current total harmonic distortion (Vthd, Ithd), active power (PowerP), apparent power (PowerS), non-active/reactive power (PowerN), true and displacement power factor (PfFwdRev, dPfFwdRev), and supply frequency. Table I summarizes the descriptive statistics of the principal electrical quantities.

B. Feature Engineering

Four domain-informed indicators were derived from the raw per-phase fields to compress the 40-field record into interpretable health metrics:

1) Current and Voltage Imbalance: computed as the standard deviation across the three phase RMS currents (Irms_A, Irms_B, Irms_C) and phase RMS voltages (Vrms_AN, Vrms_BN, Vrms_CN), respectively, capturing asymmetry between phases that is often an early indicator of winding degradation, loose connections, or single-phasing risk.

2) Average Harmonic Distortion: the per-phase current and voltage THD values were averaged to yield a single Avg_Ithd and Avg_Vthd summary metric per sample, tracking overall waveform quality against IEEE Std 519 guidance [8].

3) Calculated Power Factor: obtained as the ratio of total active power to total apparent power, PF = PowerP_Total / PowerS_Total, providing a direct, load-independent efficiency indicator.

4) Reactive Power Ratio: the ratio of total non-active power to total apparent power, PowerN_Total / PowerS_Total, used as a secondary indicator of motor magnetization health and reactive loading.

C. Statistical Process Control

A Shewhart-type individuals control chart was constructed for the engineered current-imbalance metric. The centerline was set at the sample mean, with upper and lower control limits (UCL, LCL) placed at three sample standard deviations from the mean (LCL floored at zero, since imbalance cannot be negative). Samples exceeding the UCL are flagged as statistically anomalous and warrant engineering follow-up.

D. Dimensionality Reduction and Unsupervised Clustering

The four engineered features most sensitive to operating condition — active power, current imbalance, average current THD, and calculated power factor — were standardized (zero mean, unit variance) and passed to k-means clustering with k = 3, chosen to separate normal, high-load, and transient/anomalous regimes without requiring labelled fault data [9]. Principal component analysis was applied to the same standardized feature matrix for two-dimensional visualization of the resulting clusters [10].

© AUG 2026 | IRE Journals | Volume 10 Issue 2 | ISSN: 2456-8880
DOI: https://doi.org/10.64388/IREV10I2-1722203

TABLE I. Descriptive Statistics of Principal Electrical Quantities (n = 100)

Quantity	Mean	Std. Dev.	Min	Max
Active power, PowerP_Total (W)	35,607.7	6,715.3	2,360.4	42,936.0
Apparent power, PowerS_Total (VA)	50,195.1	9,366.2	4,135.3	63,059.0
Calculated power factor	0.707	0.032	0.525	0.734
Current imbalance (A)	5.80	5.91	1.94	22.46
Voltage imbalance (V)	0.201	0.041	0.170	0.391
Avg. current THD (%)	4.85	11.52	2.18	61.01
Avg. voltage THD (%)	0.963	0.011	0.951	1.019
Frequency (Hz)	50.413	0.067	50.328	50.669

IV. RESULTS AND DISCUSSION

The engineered indicators and unsupervised analyses were computed on the full 100-sample trend record. Table I reports descriptive statistics for the principal electrical quantities; Table II reports the centroid profile of each k-means operating state. Figs. 1–7 present the corresponding visual analyses.

A. Temporal Load Profile

Fig. 1 overlays total active power against phase-A current across the monitoring window. The system exhibits a sharp inrush during start-up, followed by a cyclic steady-state load pattern with active power oscillating around a mean of 35,607.7 W (σ = 6,715.3 W) against an apparent power mean of 50,195.1 VA (σ = 9,366.2 VA), before a controlled ramp-down toward the end of the record. The repeating oscillatory envelope visible in both traces is consistent with a duty-cycling dosing or lift regime rather than a constant-speed continuous draw.

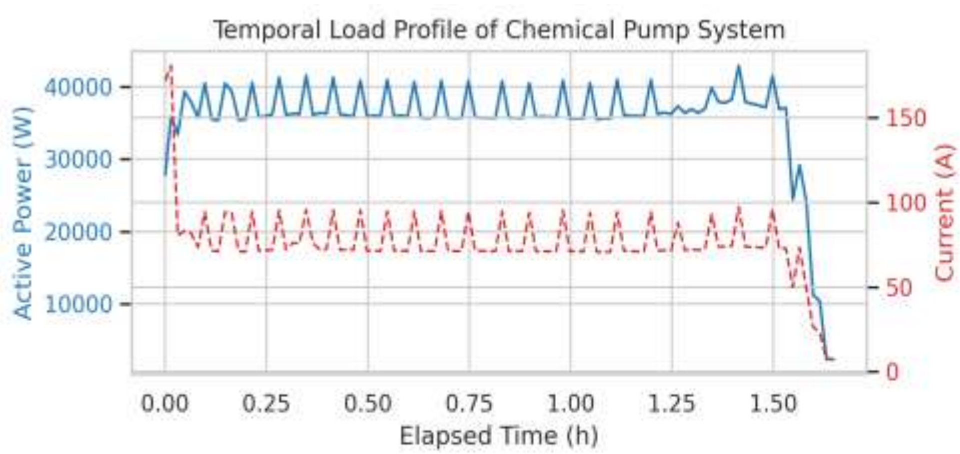

Fig. 1. Temporal load profile: active power (left axis) and phase-A current (right axis) over the monitoring window.

B. Three-Phase Current Balance

Fig. 2 traces the three individual phase currents, with the marker colour encoding the instantaneous current-imbalance magnitude. The mean current imbalance across the record is 5.80 A (σ = 5.91 A), with a maximum observed value of 22.46 A, concentrated at the start-up transient and at a small number of mid-run load excursions where phase currents visibly diverge. Steady-state operation away from these transients shows tight three-phase tracking, indicating a healthy winding/connection condition for the majority of the monitored window.

© AUG 2026 | IRE Journals | Volume 10 Issue 2 | ISSN: 2456-8880
DOI: https://doi.org/10.64388/IREV10I2-1722203

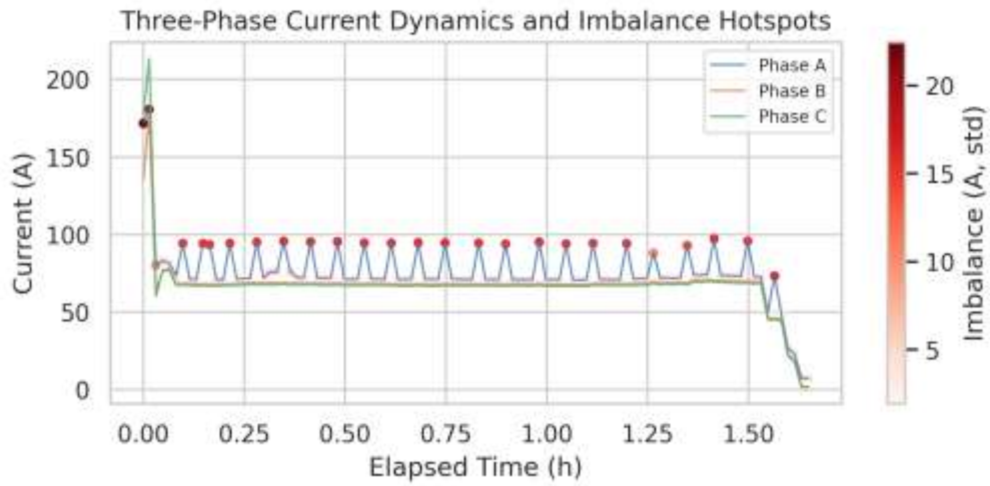

Fig. 2. Three-phase current dynamics; marker colour encodes instantaneous current-imbalance magnitude.

C. Power Quality (THD) Distribution

Fig. 3 presents the per-phase voltage and current THD distributions. Voltage THD is tightly clustered just under 1% across all three phases (mean of the phase-averaged Avg_Vthd = 0.963%, σ = 0.011%), well within the IEEE Std 519 voltage-distortion guidance for systems below 1 kV [8]. Current THD is markedly more dispersed (mean Avg_Ithd = 4.85%, σ = 11.52%), with a small number of outliers reaching above 60% during the low-current start-up/shutdown transients — a pattern typical of harmonic amplification when the fundamental current component is small relative to the switching/inrush harmonic content.

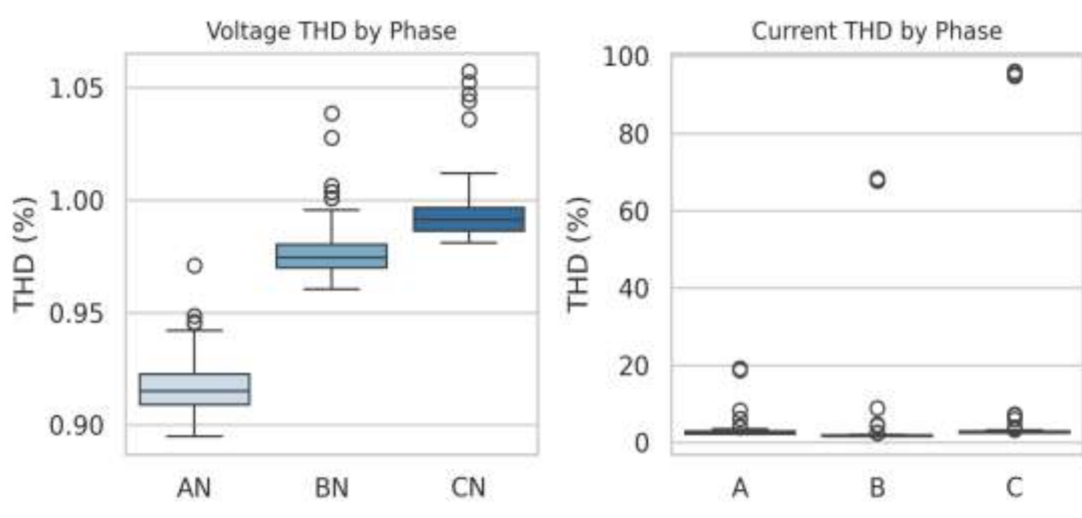

Fig. 3. Per-phase voltage THD (left) and current THD (right) distributions.

D. Power Factor and Efficiency Mapping

Fig. 4 maps active against apparent power, coloured by calculated power factor. The calculated PF averages 0.707 (σ = 0.032) across the record, ranging from 0.525 to 0.734, and the operating cloud sits consistently between the PF = 0.8 and PF = 1.0 reference lines, indicating the pump motor operates with a persistently sub-optimal but stable power factor rather than a degrading one — a condition that would benefit from power-factor-correction capacitors but does not by itself indicate an emerging fault.

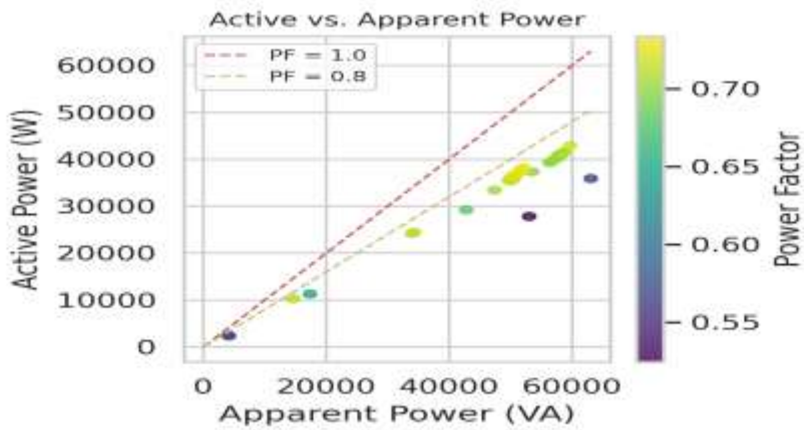

Fig. 4. Active vs. apparent power colored by calculated power factor, with PF = 1.0 and PF = 0.8 reference lines.

E. Correlation Analysis

Fig. 5 shows the pairwise correlation matrix of the key indicators. Active and apparent power are, as expected, almost perfectly correlated (r = 0.98). Notably, average current THD correlates strongly and negatively with active power (r = −0.78) and with calculated power factor (r = −0.75), confirming that harmonic distortion in this system is predominantly a light-load phenomenon rather than a persistent equipment defect. Average voltage THD correlates positively with supply frequency (r = 0.80) and current THD (r = 0.74), while current imbalance shows only weak correlation with the other indicators (|r| ≤ 0.40), suggesting imbalance behaves as a largely independent fault dimension that would not be detected by monitoring power quality or loading alone — reinforcing the value of tracking it as a separate indicator.

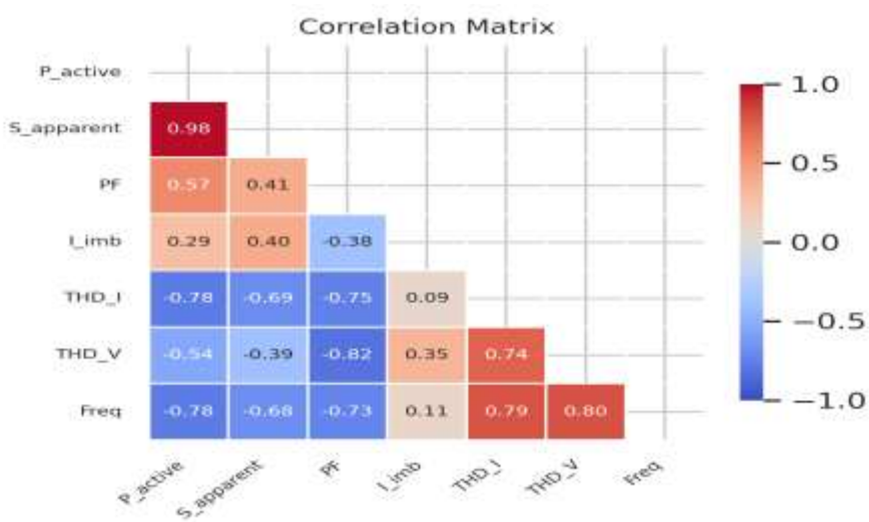

Fig. 5. Correlation matrix of key electrical health indicators.

F. Operational State Clustering

Applying PCA to the standardized feature set retained 91.7% of total variance in two components (PC1 = 60.2%, PC2 = 31.5%). K-means clustering on the same feature space (Fig. 6) partitioned the 100 samples into three operational states, summarized in Table II: a dominant steady-state regime (State 1, n = 71) characterized by moderate active power, low current imbalance, and comparatively high power factor; a high-load/imbalance regime (State 0, n = 25) with the highest active power but markedly elevated current imbalance (mean 15.25 A, roughly 6.5× the

© AUG 2026 | IRE Journals | Volume 10 Issue 2 | ISSN: 2456-8880
DOI: https://doi.org/10.64388/IREV10I2-1722203

steady-state value); and a small transient/anomalous cluster (State 2, n = 4) corresponding to the start-up/shutdown window, marked by sharply reduced active power, severely elevated current THD (mean 60.86%), and the lowest power factor observed in the dataset (0.593). This three-state partition is consistent with the physical narrative already visible in Figs. 1–4 and demonstrates that unsupervised clustering on a handful of engineered electrical features can automatically recover operationally meaningful regimes without labeled fault examples.

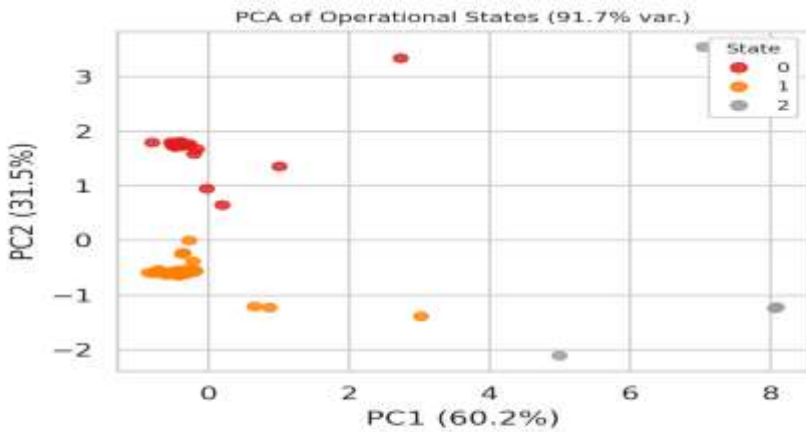

Fig. 6. PCA biplot of k-means operational states (2 components, 91.7% variance explained).

TABLE II. K-Means Operational State Centroids

Operational State	Active Power (W)	Curr. Imbalance (A)	Avg. I-THD (%)	Calc. PF
State 1 — Steady-state (n = 71)	35,542.3	2.35	2.43	0.716
State 0 — High-load/imbalance (n = 25)	39,774.9	15.25	2.73	0.699
State 2 — Transient/anomalous (n = 4)	10,724.3	7.93	60.86	0.593

G. SPC Chart for Phase Current Imbalance

Fig. 7 presents the SPC chart for current imbalance, with UCL = 23.53 A and LCL = 0 A (three-sigma limits). No individual sample exceeded the UCL over the monitored window, indicating the process remained in statistical control throughout, including the high-load/imbalance cluster identified in Section IV-F. The high-load samples nonetheless sit close to the upper control boundary (up to 22.46 A against a 23.53 A limit), and would be the first to trigger the chart under a modest further increase in loading or a genuine developing fault — illustrating the chart's practical utility as an early-warning boundary rather than only a retrospective anomaly detector.

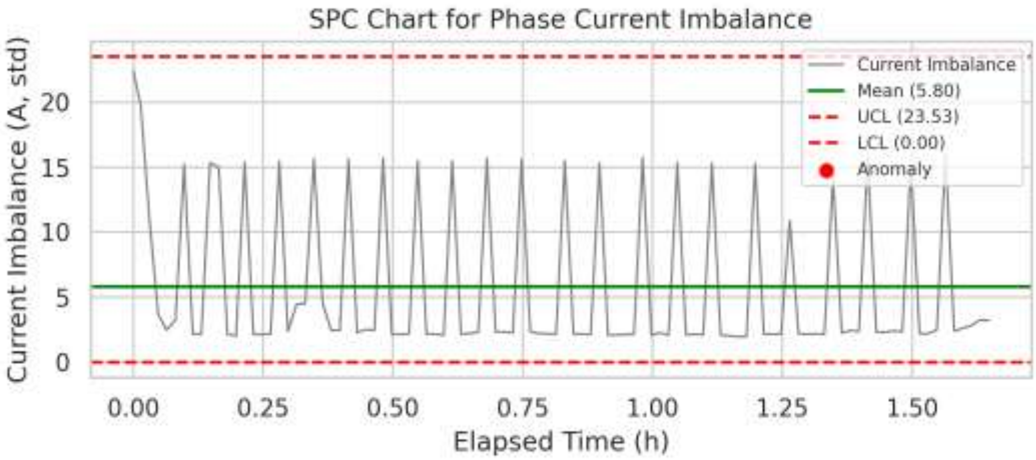

Fig. 7. Statistical process control chart for phase current imbalance (3σ limits).

V. CONCLUSION

This paper presented a multi-dimensional electrical signature analysis framework for performance monitoring and fault detection in an industrial chemical/low-lift pump system, using only routinely logged three-phase power-analyser trend data. By engineering four interpretable health indicators- current/voltage imbalance, average harmonic distortion, calculated power factor, and reactive power ratio- from raw voltage, current, THD, and power fields, the framework was able to characterize the pump's operating behaviour without requiring additional vibration or acoustic sensing. Statistical process control identified a stable operating envelope for phase current imbalance across the monitored window, while unsupervised PCA/k-means clustering, retaining 91.7% of feature variance in two components, automatically separated the data into a dominant steady-state regime, a high-load/imbalance regime, and a transient start-up/shutdown regime whose electrical signature (severely elevated current THD and depressed power factor) matches physical expectation.

The correlation analysis further showed that, in this system, current harmonic distortion is predominantly a function of loading rather than an independent fault signature, whereas current imbalance behaves largely independently of loading and power quality — underscoring the need to track it separately rather than infer it from other electrical quantities. These findings suggest that low-cost, non-invasive electrical signature analysis, combined with simple and interpretable statistical and unsupervised machine-learning techniques, can provide plant engineers with a practical early-warning capability for chemical and low-lift pump systems. Future work will extend the monitored window to capture confirmed fault events, validate the SPC and clustering thresholds against maintenance records, and evaluate supervised classification once labeled fault data become available.

ACKNOWLEDGMENT

The authors thank the plant instrumentation and maintenance personnel who facilitated access to the power-analyzer trend logs used in this study.

REFERENCES

[1] G. B. Kliman, R. A. Koegl, J. Stein, R. D. Endicott, and M. W. Madden, "Noninvasive detection of broken rotor bars in operating induction motors," IEEE Trans. Energy Convers., vol. 3, no. 4, pp. 873–879, Dec. 1988.

[2] S. Nandi, H. A. Toliyat, and X. Li, "Condition monitoring and fault diagnosis of electrical motors—A review," IEEE Trans. Energy Convers., vol. 20, no. 4, pp. 719–729, Dec. 2005.

© AUG 2026 | IRE Journals | Volume 10 Issue 2 | ISSN: 2456-8880
DOI: https://doi.org/10.64388/IREV10I2-1722203

[3] G. Niu, X. Dong, and Y. Chen, "Motor fault diagnostics based on current signatures: A review," IEEE Trans. Instrum. Meas., vol. 72, pp. 1–19, 2023.

[4] S. Halder, S. Bhat, D. Zychma, and P. Sowa, "Broken rotor bar fault diagnosis techniques based on motor current signature analysis for induction motor—A review," Energies, vol. 15, no. 22, art. 8569, 2022.

[5] V. Becker, T. Schwamm, S. Urschel, and J. A. Antonino-Daviu, "Fault detection of circulation pumps based on motor current evaluation," IEEE Trans. Ind. Appl., vol. 57, no. 5, pp. 4617–4624, 2021.

[6] V. Becker, T. Schwamm, S. Urschel, and J. A. Antonino-Daviu, "Two current-based methods for the detection of bearing and impeller faults in variable speed pumps," Energies, vol. 14, no. 15, art. 4514, 2021.

[7] C. E. Sunal, V. Velisavljevic, V. Dyo, B. Newton, and J. Newton, "Centrifugal pump fault detection with convolutional neural network transfer learning," Sensors, vol. 24, no. 8, art. 2442, 2024.

[8] IEEE Std 519-2014, IEEE Recommended Practice and Requirements for Harmonic Control in Electric Power Systems, IEEE, Piscataway, NJ, USA, 2014.

[9] J. MacQueen, "Some methods for classification and analysis of multivariate observations," in Proc. 5th Berkeley Symp. Math. Stat. Probab., vol. 1, 1967, pp. 281–297.

[10] I. T. Jolliffe, Principal Component Analysis, 2nd ed. New York, NY, USA: Springer, 2002.